Identification of Suitable Managed Aquifer Recharge Sites Using GIS-AHP and Field-Based Evaluation of Aquifer Storage Capacity in Central Kazakhstan

Abai Jabassov , Zhuldyzbek Onglassynov * , Aigerim Alimgazina , Vladimir Smolyar , Arai Ermenbay , Daniil Ereev , Raushan Amanzholova

Posted Date: 23 April 2026

doi: 10.20944/preprints202604.1713.v1

Keywords: groundwater recharge; groundwater balance; managed aquifer recharge; groundwater monitoring; analytic hierarchy process; remote sensing; GIS

 doi:10.20944/preprints202604.1713.v1

Article

Identification of Suitable Managed Aquifer Recharge Sites Using GIS-AHP and Field-Based Evaluation of Aquifer Storage Capacity in Central Kazakhstan

Abai Jabassov [1], Zhuldyzbek Onglassynov [1,*], Aigerim Alimgazina [1], Vladimir Smolyar [1], Arai Ermenbay [1], Daniil Ereev [1] and Raushan Amanzholova [2]

[1] Ahmedsafin Institute of Hydrogeology and Environmental Geosciences, Satbayev University, Almaty 050010, Kazakhstan

[2] Kazakh-British Technical University, Almaty 050000, Kazakhstan

* Correspondence: zh.onglassynov@satbayev.university

Abstract

Managed aquifer recharge (MAR) is increasingly being realized as an important approach to improve water security in arid and semi-arid environments where there is a low amount of sur-face water and high climatic variability. This paper introduces a unified approach to the process of locating appropriate MAR locations and estimating recharge potential in Central Kazakhstan through the multi-criteria analysis using GIS and hydrogeological field exploration, water balance modelling. The suitability testing was preliminarily performed in the Google Earth Engine environment as a weighted overlay test with the combination of terrain, vegetation, hydrological, and land cover parameters. According to the suitability map obtained and patterns of activity in agricultural activities, eleven candidate sites were identified out of which eight were found to be suitable after hydrochemical analysis. The Nesterov and Boldyrev techniques of field-based infiltration tests, produced a range of 0.05 to 1.42 m/day of hydraulic conductivity. Water balance analysis shows that the total amount of water that could be recharged into the suitable sites is about 40.2 million m^3/year and that the effective amount of water could be recharged is about 11.0 million m^3/year, which is limited by the infiltration processes. This means that about 27 percent of the available water is added into ground water recharge which is a significant boost to the original estimates. The assessment of the storage capacity of the aquifers indicates that at all locations, the pore space is much greater than the recharge volumes that have been calculated and, therefore, storage is not a limiting factor in the implementation of MAR. It is estimated that there are recharge rates of between 174 and 5,282 m^3/day, with a high degree of spatial variability which is caused by local hydrogeological circumstances. The suggested method offers a powerful and generalizable site selection and measurement framework of MAR in arid areas with limited data. The findings highlight the significance of combining remote sensing, field measurements, and process-based modeling to aid sustainable groundwater management and climate adaptation strategies.

Keywords: groundwater recharge; groundwater balance; managed aquifer recharge; groundwater monitoring; analytic hierarchy process; remote sensing; GIS

1. Introduction

In the context of increasing water scarcity in arid and semi-arid regions of the world—driven by climate change, population growth, and intensive agricultural activities—Managed Aquifer Recharge (MAR) technologies are gaining strategic importance for ensuring water security. MAR represents a set of engineering and management measures aimed at enhancing groundwater reserves through the deliberate infiltration or injection of surplus surface water, treated wastewater, or desalinated water into the most reliable natural reservoir—aquifers. MAR is particularly important

 doi:10.20944/preprints202604.1713.v1

for agriculture in arid regions, where precipitation is unevenly distributed, surface runoff is highly seasonal, and irrigation systems are strongly dependent on surface water sources.

This literature review, based on the analysis of more than 30 scientific studies, systematizes current approaches, methodologies, results, and regional experiences in the application of Managed Aquifer Recharge (MAR), with particular emphasis on arid conditions and a comparative analysis of international and post-Soviet practices. A key stage in MAR planning is the identification and suitability assessment of potential sites, for which geographic information systems (GIS) and multi-criteria decision analysis methods are widely applied.

Studies conducted in Qatar [1], India [10], China [11], and the Ganges Basin [12] demonstrate the effectiveness of integrating GIS, remote sensing, and criteria-weighting methods such as the Analytical Hierarchy Process (AHP) and its fuzzy extensions (FAHP), enabling the development of highly reliable recharge potential maps [10, 11, 12, 15]. Hydrological and hydrogeological models are активно used for forecasting outcomes and optimizing technical schemes, as illustrated by the application of SWAT in Tunisia [2] and integrated isotope and tracer modeling in karst systems in China [3].

A modern trend is the adoption of artificial intelligence methods: hybrid deep learning and remote sensing approaches improve the accuracy of identifying suitable MAR zones [14], while global neural network models with explainable AI (XAI) help reveal complex nonlinear relationships [13]. Review studies [4] highlight universal success factors for MAR implementation, including hydrogeological parameters (e.g., transmissivity and permeability), the availability and quality of recharge water, and the management of contamination risks (e.g., clogging). These studies emphasize the importance of an integrated approach incorporating continuous monitoring and adaptive management [4, 20]. Global experience confirms the high potential of Managed Aquifer Recharge (MAR) as a tool for climate change adaptation. In the arid countries of the Persian Gulf (Qatar [1]), MAR is considered a solution to freshwater scarcity and the threat of seawater intrusion, while in North Africa [2] and South Africa [9], the focus is on the use of seasonal runoff and stormwater. In Europe (Germany [7], Switzerland [19]), localized, nature-based solutions (near-nature MAR), such as managed floodplain infiltration, are increasingly being developed due to their environmental sustainability and economic efficiency. In Turkey [5], significant historical experience has been accumulated; however, the development of MAR is constrained by institutional barriers. A common conclusion of international studies is the need to integrate MAR into national water resource management strategies [4, 5, 20].

In post-Soviet countries and Russia, interest in MAR is also high due to acute water scarcity in many arid regions, although the context and approaches have specific characteristics. Studies are often focused on addressing critical local challenges, such as aquifer depletion in urban areas (Derbent, Russia [21]) or ensuring water supply for agriculture under sharply continental climatic conditions (Aktobe region, Kazakhstan [23]; Eastern Orenburg region, Russia [24]). A number of works are devoted to adapting MAR methods to unique natural conditions, such as the use of takyr runoff in Uzbekistan [36] or integrated flow regulation along the Black Sea coast of Russia [32].

Russian-language publications particularly emphasize the role of the vadose zone as a natural filter and highlight the advantages of environmentally friendly infiltration methods [22, 27, 28], considering MAR not only as a technical solution but also as an environmental protection measure [27, 28]. The need to improve hydrogeological assessment methodologies [31] and regulatory frameworks [5, 25, 30], as well as to account for water balance dynamics [29], is also emphasized. Unlike many international studies that focus on advanced modeling techniques and artificial intelligence, research in the CIS more often prioritizes classical hydrogeological justification and adapted engineering solutions, although there is a growing convergence of approaches—for example, in the use of 3D modeling for AgMAR [33] and the incorporation of international experience [30].

Thus, the analysis of an extensive body of literature [1–36] demonstrates that MAR is widely recognized as a highly effective tool for enhancing water security in arid environments. Its successful

 doi:10.20944/preprints202604.1713.v1

implementation depends on the integrated consideration of hydrogeological conditions, the quality of recharge sources, and effective management. While international experience reflects a wide diversity of technological solutions, in the CIS and Russia the potential of MAR is realized primarily through addressing urgent regional challenges, with an emphasis on environmental safety and the adaptation of classical engineering approaches. This highlights the importance of integrating advanced global practices with in-depth regional analysis to ensure the sustainable development of water-scarce territories.

2. Materials and Methods

2.1. Study Area

Central Kazakhstan (Figure 1) is characterized by an arid climate, pronounced seasonality of precipitation, limited surface water resources, and a complex hydrogeological structure. Under such conditions, identifying suitable sites for Managed Aquifer Recharge (MAR) requires comprehensive spatial analysis. For these tasks, one of the most justified and widely applied approaches is the Weighted Overlay method within Geographic Information Systems (GIS).

Figure 1. Study area location.

The Weighted Overlay method enables the integration of heterogeneous spatial datasets, including lithology, topography, groundwater depth, permeability of geological formations, climatic parameters, and hydrological characteristics. Each factor is standardized and assigned a weight coefficient according to its influence on infiltration processes and natural aquifer recharge. As a result, a final suitability map is generated, reflecting the spatial distribution of areas with varying potential for MAR implementation.

The effectiveness of this approach has been confirmed by numerous studies conducted in arid and semi-arid regions that are climatically and geologically comparable to Central Kazakhstan. The scientific literature demonstrates that the use of multi-criteria decision analysis (MCDA) methods, including Weighted Overlay and the Analytic Hierarchy Process (AHP), provides robust and

 doi:10.20944/preprints202604.1713.v1

reproducible results in mapping groundwater recharge zones. In several studies, modeling results were successfully validated against observed groundwater level data, confirming the practical applicability of the method.

For Central Kazakhstan, this approach is particularly relevant, as it allows for the consideration of spatial heterogeneity in geological conditions, variations in rock permeability, and differences in climatic parameters. The application of the Weighted Overlay method enables the integration of large volumes of geospatial data into a unified analytical model, facilitating the well-grounded selection of suitable sites for artificial aquifer recharge and the planning of sustainable water resource management measures.

2.2. Methodology of Research

As a result of applying the Weighted Overlay method, an integrated suitability map for MAR implementation areas was generated using the Google Earth Engine (GEE).

A preliminary MAR suitability assessment was implemented in the Google Earth Engine (GEE) environment using a multi-criteria spatial approach. The model integrates terrain, vegetation, precipitation, drainage, and land cover parameters derived from global datasets. Each factor was transformed to a dimensionless suitability scale (0–1) and combined using a weighted linear combination defined through model parameters. Areas with suitability values exceeding the predefined threshold were classified as potential MAR zones.

- Input data and calculation methods

Terrain slope was derived from the SRTM digital elevation model (USGS/SRTMGL1_003) and converted to percent. Suitability was calculated using a trapezoidal function with thresholds defined in the model parameters (Figure 2).

```
var dem = ee.Image('USGS/SRTMGL1_003').clip(AOI);
var slopePct = ee.Terrain.slope(dem).tan().multiply(100).rename('slope_pct');

var slopeSuit = trapezoidSuitability(
  slopePct,
  params.slopeHardMin,
  params.slopeIdealMin,
  params.slopeIdealMax,
  params.slopeHardMax
).rename('S_slope');
```

Figure 2. Derivation of terrain slope from SRTM DEM using a trapezoidal membership function.

Vegetation conditions were assessed using Sentinel-2 Surface Reflectance Harmonized imagery (COPERNICUS/S2_SR_HARMONIZED) within the time range defined in the model parameters. NDVI was calculated from a median composite after cloud masking using the SCL band (Figure 3).

```
var s2 = ee.ImageCollection('COPERNICUS/S2_SR_HARMONIZED')
  .filterBounds(AOI)
  .filterDate(params.ndviStart, params.ndviEnd)
  .map(maskS2sr);

var ndvi = s2.median().clip(AOI).normalizedDifference(['B8', 'B4']).rename('NDVI');
var ndviSuit = trapezoidSuitability(
  ndvi,
  0.05,  // hardMin
  0.12,  // a
  0.40,  // b
  0.65   // hardMax
).rename('S_ndvi');
```

Figure 3. Assessment of vegetation conditions using NDVI derived from Sentinel-2 data with normalization applied.

 doi:10.20944/preprints202604.1713.v1

Precipitation conditions were estimated using the CHIRPS daily dataset (UCSB-CHG/CHIRPS/DAILY) for the period specified in the parameters. Mean annual precipitation was calculated and normalized within the AOI (Figure 4, Figure 24 b).

```
var chirps = ee.ImageCollection('UCSB-CHG/CHIRPS/DAILY')
  .filterBounds(AOI)
  .filterDate(params.rainStart, params.rainEnd);

var rainAnnual = chirps.select('precipitation').mean().multiply(365)
  .rename('P_annual_mm')
  .clip(AOI);

var rainStats = rainAnnual.reduceRegion({
  reducer: ee.Reducer.minMax(),
  geometry: AOI.geometry(),
  scale: 5000,
  bestEffort: true,
  maxPixels: 1e13
});

var rainMin = ee.Number(rainStats.get('P_annual_mm_min'));
var rainMax = ee.Number(rainStats.get('P_annual_mm_max'));
var rainSuit = norm01(rainAnnual, rainMin, rainMax).rename('S_rain');
```

Figure 4. Estimation of mean annual precipitation based on CHIRPS data and its normalization for suitability analysis.

Drainage conditions were derived from the HydroSHEDS FreeFlowingRivers dataset (WWF/HydroSHEDS/v1/FreeFlowingRivers). The river network was rasterized and analyzed within a moving window defined by the model parameters (Figure 5).

```
var rivers = ee.FeatureCollection('WWF/HydroSHEDS/v1/FreeFlowingRivers')
  .filterBounds(AOI);

print('Rivers count in AOI:', rivers.size());
Map.addLayer(rivers, {color: 'cyan'}, 'Rivers (HydroSHEDS)', false);

var riversRaster = ee.Image(0).byte().paint({
  featureCollection: rivers,
  color: 1,
  width: 1
}).rename('rivers').clip(AOI);

var scaleM = 250;
var kernel = ee.Kernel.circle({radius: params.densityRadiusM, units: 'meters', normalize: false});

var lineCount = riversRaster.reduceNeighborhood({
  reducer: ee.Reducer.sum(),
  kernel: kernel
});
var lineLen_m = lineCount.multiply(scaleM);

var pxCount = ee.Image(1).reduceNeighborhood({
  reducer: ee.Reducer.sum(),
  kernel: kernel
});
var area_m2 = pxCount.multiply(scaleM * scaleM);

var drainDen = lineLen_m.divide(area_m2)
  .multiply(1e6)
  .divide(1000)
  .rename('DrainDen')
  .clip(AOI);

var ddPct = drainDen.reduceRegion({
  reducer: ee.Reducer.percentile([20, 50, 80]),
  geometry: AOI.geometry(),
  scale: scaleM,
  bestEffort: true,
  maxPixels: 1e13,
  tileScale: 4
});
```

Figure 5. Derivation of drainage conditions based on the HydroSHEDS FreeFlowing Rivers dataset using neighborhood analysis.

Land cover suitability was derived from ESA WorldCover (ESA/WorldCover/v200/2021) by assigning predefined suitability values (Figure 6).

 doi:10.20944/preprints202604.1713.v1


```
var wc = ee.Image('ESA/WorldCover/v200/2021').select('Map').clip(AOI);

var lulcSuit = ee.Image(0)
  .where(wc.eq(30), 0.90) // Grassland
  .where(wc.eq(20), 0.80) // Shrubland
  .where(wc.eq(60), 0.55) // Bare/sparse (not 1.0!)
  .where(wc.eq(40), 0.50) // Cropland
  .where(wc.eq(10), 0.25) // Tree cover
  .where(wc.eq(90), 0.20) // Wetland
  .where(wc.eq(50), 0.00) // Built-up
  .where(wc.eq(80), 0.00) // Permanent water
  .where(wc.eq(70), 0.00) // Snow/ice
  .where(wc.eq(95), 0.00) // Mangroves
  .where(wc.eq(100),0.00) // Moss/lichen
  .rename('S_lulc');

Map.addLayer(wc, {}, 'WorldCover LULC', false);
Map.addLayer(lulcSuit, {min: 0, max: 1}, 'S_lulc (CZ tuned)', false);
```

Figure 6. Land cover suitability classification based on ESA WorldCover data with assigned suitability scores.

The final MAR suitability index was calculated using the weighted linear combination defined in the model parameters (Figure 7):

```
var suitability = slopeSuit.multiply(params.wSlope)
  .add(ndviSuit.multiply(params.wNDVI))
  .add(rainSuit.multiply(params.wRain))
  .add(drainSuit.multiply(params.wDrain))
  .add(lulcSuit.multiply(params.wLULC))
  .rename('MAR_suitability')
  .clip(AOI);

var potential = suitability.gte(params.suitabilityThreshold).selfMask().rename('Potential_MAR');
```

Figure 7. Final MAR suitability index calculated using the weighted linear combination of model parameters.

This map illustrates the spatial distribution of the potential for Managed Aquifer Recharge (MAR) across the territory of Central Kazakhstan (Figure 8).

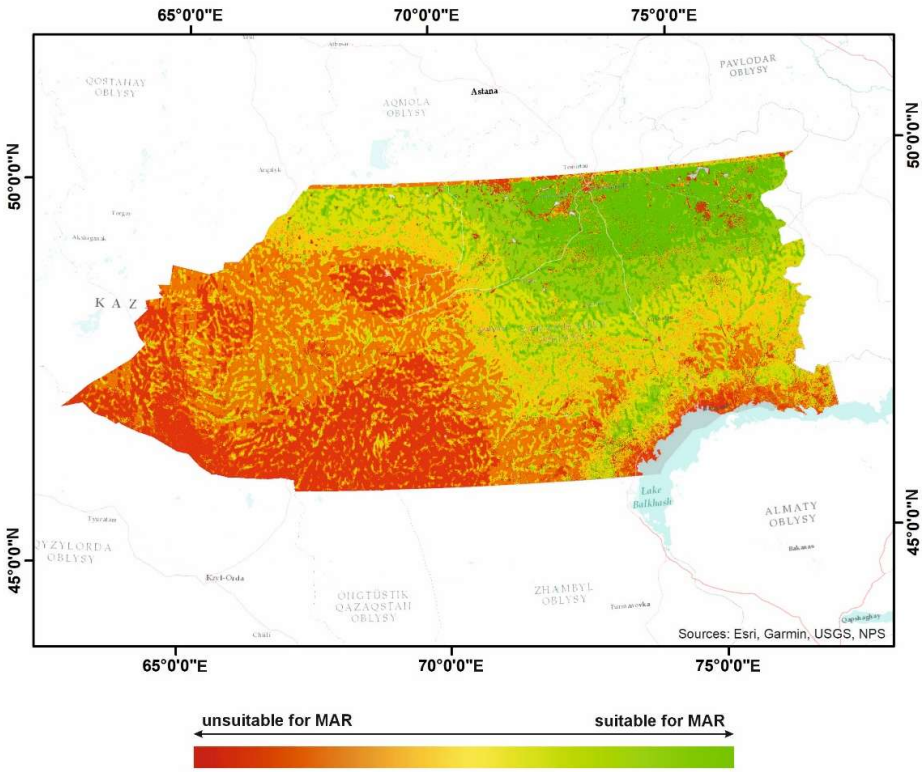

Figure 8. Spatial distribution of MAR suitability potential across Central Kazakhstan.

 doi:10.20944/preprints202604.1713.v1

The color scale ranges from red and orange shades (low suitability) to green shades (high suitability). Red areas are characterized by unfavorable conditions for MAR, which may be associated with low rock permeability, steep surface slopes, limited infiltration capacity, or unfavorable hydrogeological conditions. Green areas indicate the most promising sites. These territories are characterized by a combination of favorable factors, including relatively gentle terrain, higher filtration capacity of rocks, suitable groundwater depth, and conditions that promote the accumulation and infiltration of surface runoff. Such zones represent areas with high potential for the placement of MAR infrastructure.

Based on Figure 8, watershed areas with the highest potential for MAR implementation were identified. Their spatial distribution indicates a concentration of promising sites in zones that combine a well-developed river network, moderate surface slopes, and favorable filtration properties of geological formations (Figure 9).

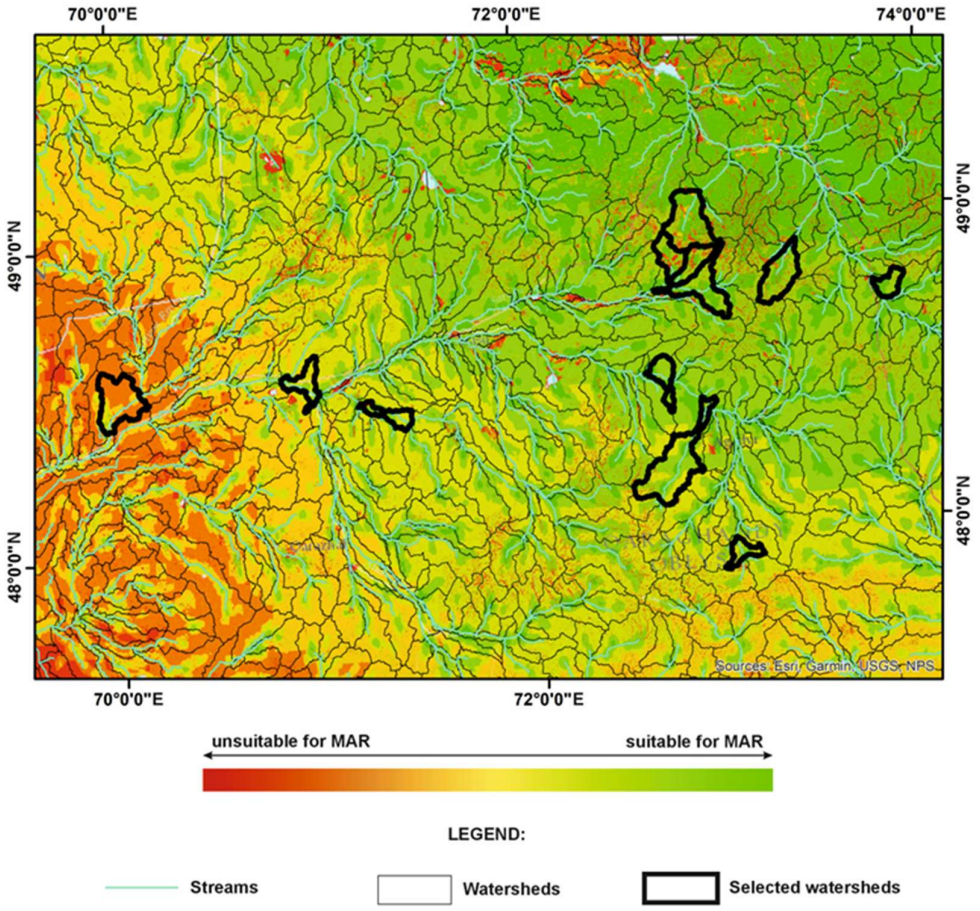

Figure 9. Detailed analysis of selected watersheds with drainage network and MAR suitability overlay.

These areas were selected based on the presence of agricultural activity (Figure 10). The selection is based on the spatial alignment of these areas with zones of active agricultural use, as delineated by the green dashed outline on the map. Agricultural areas are characterized by an increased demand for water resources, particularly under the arid and semi-arid climate conditions of Central Kazakhstan. Intensive irrigation and groundwater exploitation in such regions often lead to declining groundwater levels, the development of water scarcity, and an increased risk of land degradation.

Therefore, agricultural areas represent priority zones for the implementation of MAR measures aimed at stabilizing the water balance and enhancing the sustainability of agro-landscapes (Figure 10).

 doi:10.20944/preprints202604.1713.v1

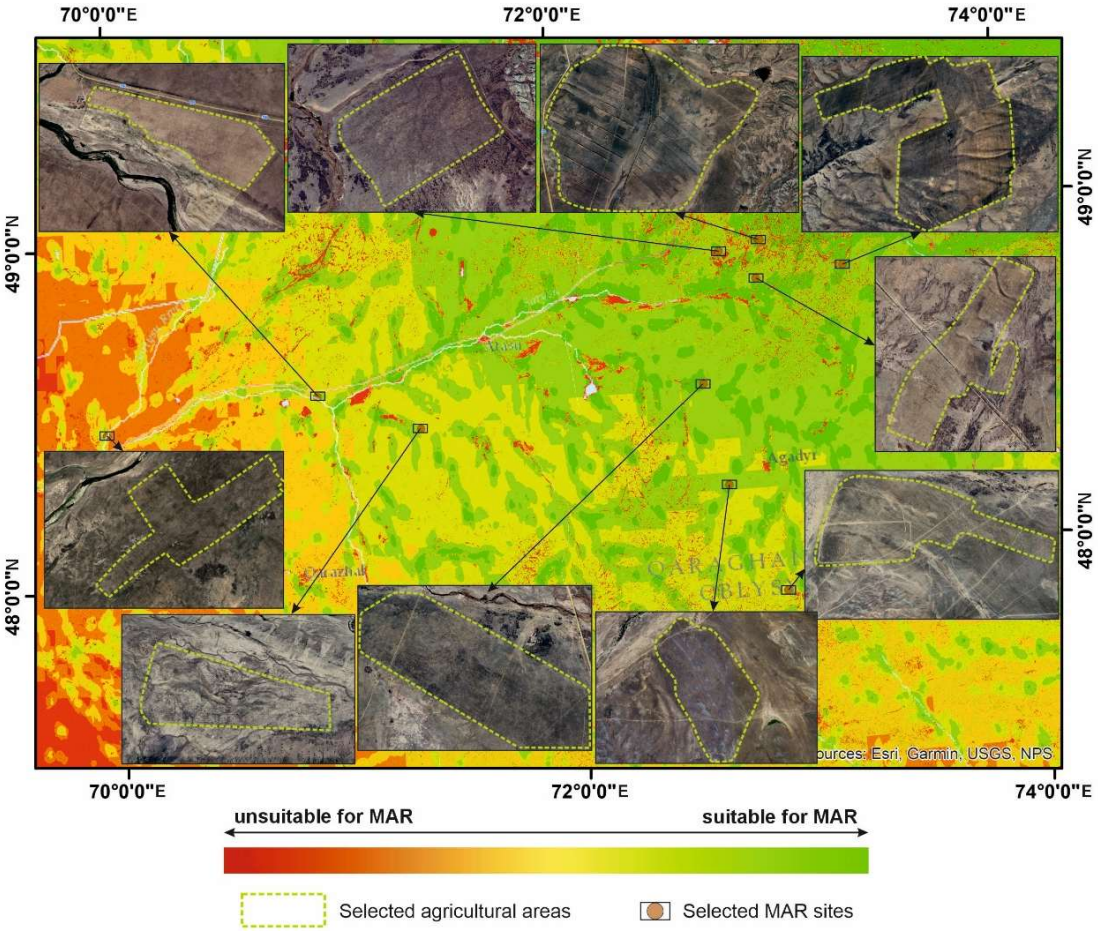

Figure 10. Spatial distribution of selected agricultural areas in relation to MAR suitability zones, with representative site examples.

In addition, the selected sites are located within watersheds with a well-developed drainage network, which creates favorable conditions for the accumulation of surface runoff and its subsequent infiltration. The spatial coincidence of favorable natural conditions (moderate slopes, presence of streams, and potentially permeable deposits) and intensive land use further strengthens the justification for their selection.

The identified sites (Selected MAR sites) were determined not only based on the results of the weighted multi-criteria analysis but also considering the factor of active agricultural use. This ensures the practical relevance of the study and directs the proposed solutions toward the most water-scarce and socio-economically significant areas of the region.

Next, hydrogeological maps at a scale of 1:200,000 (Figure 11) were digitized to identify the presence of recharge collectors. These collectors are essential for capturing and distributing directed infiltration of surface runoff to enhance groundwater storage. In this case, the collectors are represented by modern sedimentary deposits, predominantly fluvial, which—due to their filtration properties—are considered highly suitable for MAR implementation.

 doi:10.20944/preprints202604.1713.v1

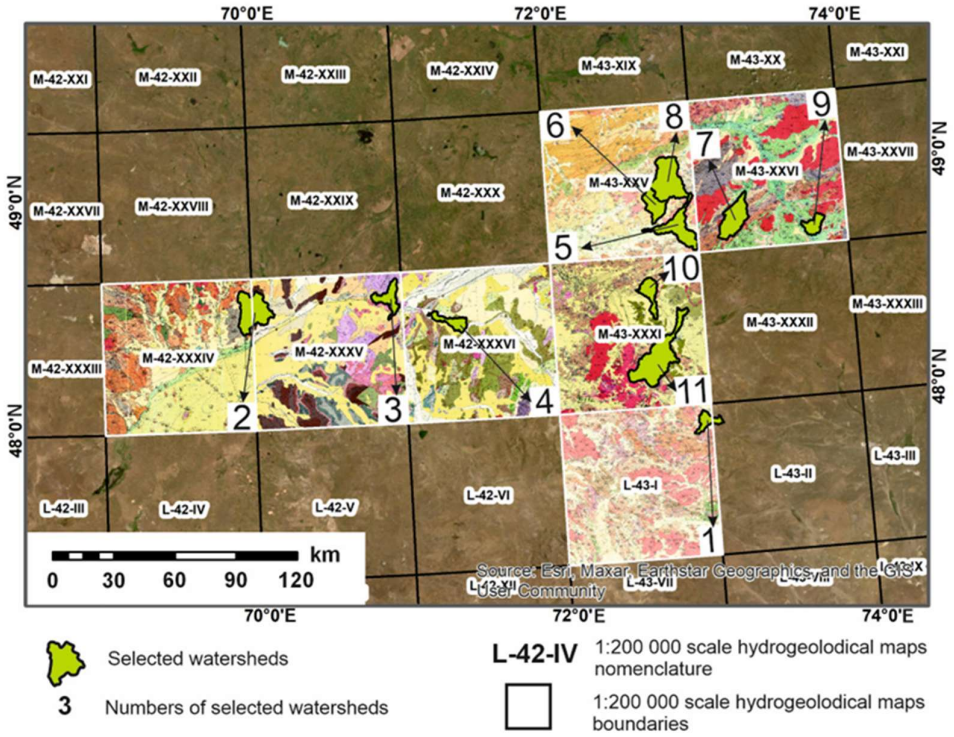

Figure 11. Digitized hydrogeological map (1:200,000 scale) used to identify recharge collectors suitable for MAR implementation.

The selected MAR sites are confirmed by hydrogeological maps (Figure 12).

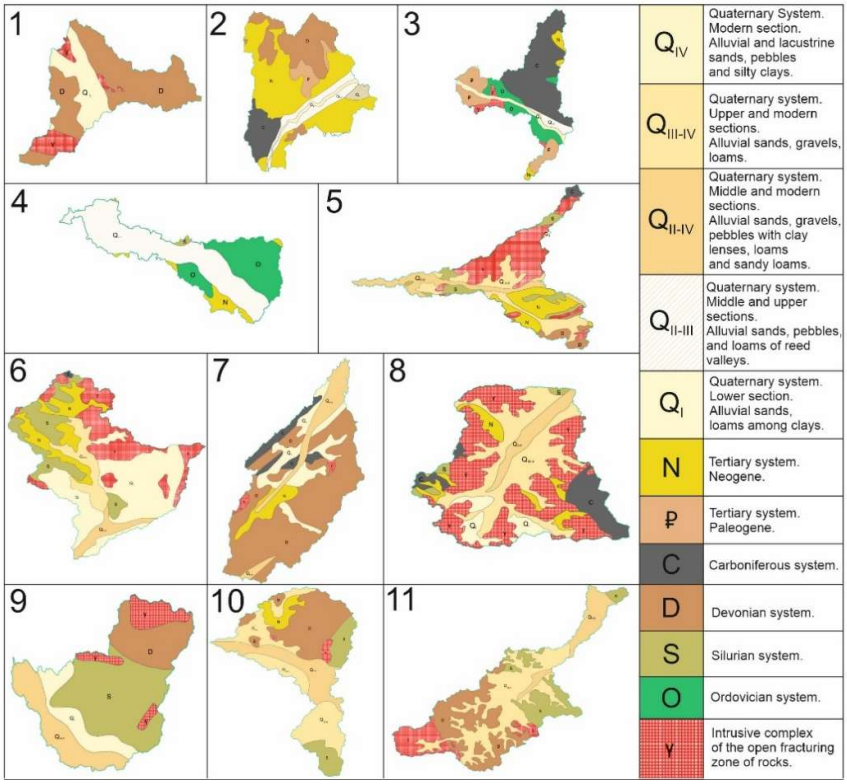

Figure 12. Hydrogeological units of selected MAR sites derived from digitized 1:200,000 scale maps.

 doi:10.20944/preprints202604.1713.v1

Overall, the maps (Figures 8–11) demonstrate a pronounced spatial differentiation of the potential for Managed Aquifer Recharge (MAR) across Central Kazakhstan and serve as a basis for further detailed hydrogeological justification of MAR site placement.

Within the framework of this study, field visits and in situ tests were conducted to determine the filtration properties of the proposed recharge collectors. These properties were evaluated using the methods developed by Nesterov and Boldyrev. The determination of the filtration coefficient (K) using these methods represents a simple and illustrative approach to assessing soil permeability directly under natural conditions. In international practice, the pit infiltration methods known in Russian literature as the Nesterov and Boldyrev methods are referred to as the single-ring (or pit) infiltration method and the double-ring infiltrometer method.

Due to their simplicity, these methods are widely used in modern hydrogeology and engineering geology and have been applied in various climatic and environmental settings, including studies conducted in China [37, 38], Canada [39], European countries [40], and the Middle East [41].

The Nesterov method is based on observing the decline of the water level in a specially drilled borehole or pit. After filling the excavation with water, the decrease in water level is recorded over time. This decline is associated with the infiltration of water into the surrounding soil. Regular measurements of the water level depth are taken at specified time intervals (e.g., every 5–10 minutes at the initial stage). Based on the resulting drawdown curve, the filtration coefficient is calculated using a formula that accounts for the diameter of the excavation, the height of the water column, and the rate of water level decline. The method is simple to apply but requires careful measurements and consideration of soil homogeneity.

The Boldyrev method is used to determine filtration properties in shallow excavations and is based on the principle of steady-state infiltration. Water is supplied to a prepared pit while maintaining a constant water level (Figure 13). The volume of water required to sustain this constant level over a given time period is measured, i.e., the discharge infiltrating into the soil under constant head conditions is recorded. The filtration coefficient is then calculated using a formula that considers the infiltration surface area, hydraulic head, and water discharge. This method is considered more robust against random errors, as it is based on steady-state flow conditions.

Both methods provide approximate values of the filtration coefficient under natural conditions without the need for complex equipment. The Nesterov method is suitable for rapid assessments and dynamic observations, whereas the Boldyrev method provides more stable estimates under constant head conditions. The obtained values are used in calculating site infiltration capacity, designing MAR facilities, and assessing soil permeability in land reclamation and water management systems.

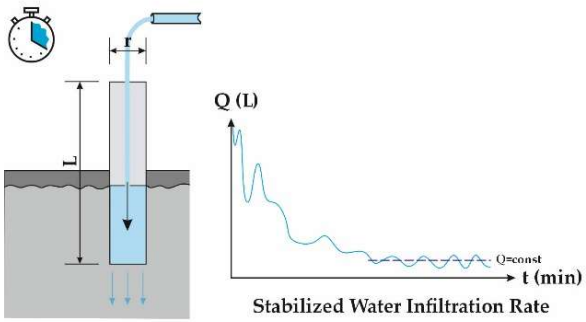

Figure 13. Conceptual scheme of infiltration testing and stabilization of infiltration rate over time.

Field investigations began with the construction of test pits: using a hand auger, boreholes up to 1.4 m deep and approximately 0.3 m in diameter were drilled at the selected sites (Figure 14). These parameters ensured a sufficient infiltration surface area and allowed tests to be conducted under natural soil conditions without significant disturbance of the soil structure.

 doi:10.20944/preprints202604.1713.v1

After preparation of the boreholes, infiltration tests were carried out using the Nesterov and Boldyrev methods. During the experiments, the dynamics of water level decline in the borehole and the volume of water infiltrating into the soil under specified head conditions were recorded (Figure 14). Regular measurements of time and water discharge were performed, which made it possible to obtain reliable data on the characteristics of the infiltration process.

Figure 14. Field experiments for determining soil infiltration properties using in situ infiltration methods.

The filtration properties of the vadose (unsaturated) zone at the selected prospective sites were determined using the pit (borehole) infiltration method in the unsaturated zone. The essence of this approach is to drill a borehole within the vadose zone and fill it with water until infiltration occurs at a constant rate. During the test, the water level is maintained constant, and the borehole parameters must satisfy the following condition:

$$12{,}5 < \frac{L}{r} < 50{,}0 \quad (1)$$

where L is the depth of the borehole into which water is introduced, and r is the borehole radius. In this study, a hand auger with a working radius of 3 cm was used. Since infiltration tests at all sites were conducted up to the borehole collar, the drilling depth—according to the above condition—had to range from 0.38 to 1.5 m.

After the experiments, graphs of the relationship between the volume of absorbed water and time were constructed. If, from a certain point onward, the measured data formed a straight line, it was assumed that infiltration had stabilized, i.e., the inflow rate (Q) became constant. The obtained value of Q was then substituted into Philip's equation [43] to calculate the filtration coefficient (k_f) of the tested unsaturated deposits:

$$k_{ф} = 0{,}423\frac{Q}{L^2}\lg\frac{2L}{r} \quad (2)$$

As a result, the filtration coefficient of the near-surface sedimentary deposits was determined to range from 0.05 to 1.42 m/day, with an average value of 0.54 m/day (Table 1, Figure 15).

The obtained values made it possible to quantitatively assess the permeability of the soils and to use these results for further hydrogeological justification of the studied sites.

 doi:10.20944/preprints202604.1713.v1

Table 1. Filtration Coefficients.

Observation point	Steady-state discharge, L/h	Borehole depth, m	Filtration coefficient (k_n), m/day
1	18.4	0.9	0.41
2	4.98	1.40	0.05
3.1	19.25	0.70	0.67
3.2	8.22	0.60	0.37
4	13.80	0.55	0.72
5	23.04	0.50	1.42
6	5.64	1.00	0.10
7	13.98	1.00	0.26
8	9.18	0.50	0.57
9	17.28	0.75	0.53
10	16.50	0.50	1.02
11	7.50	0.60	0.34

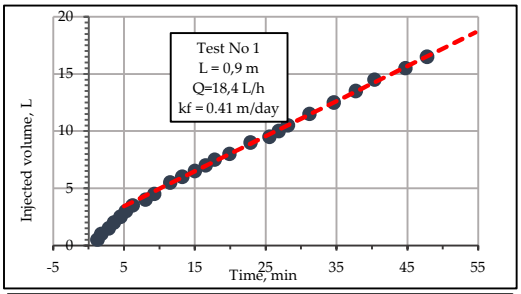

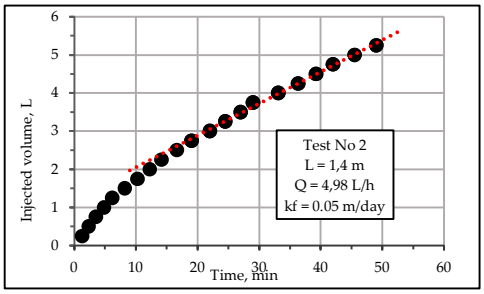

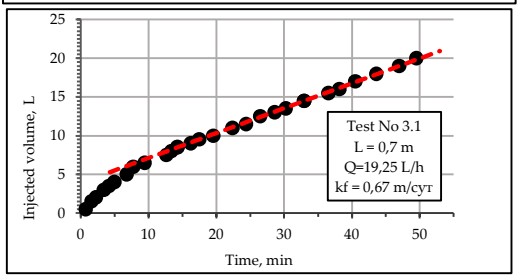

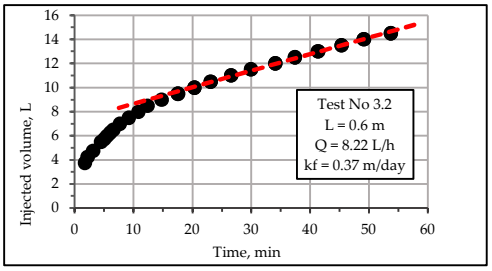

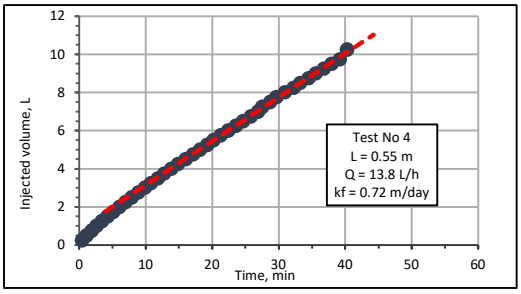

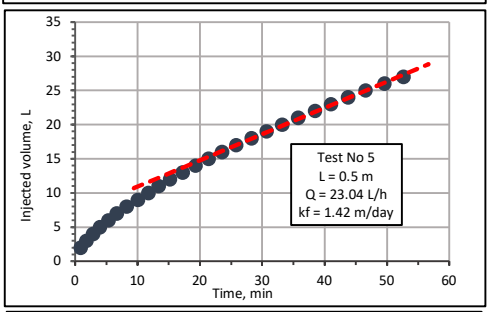

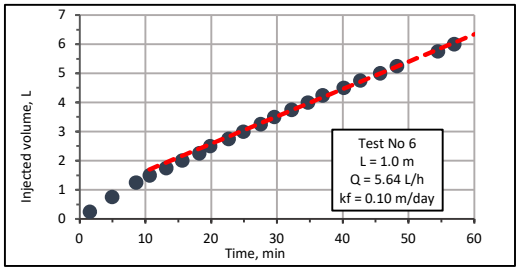

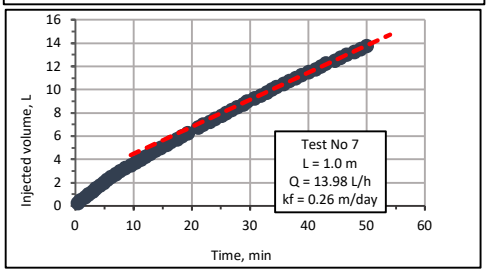

 doi:10.20944/preprints202604.1713.v1

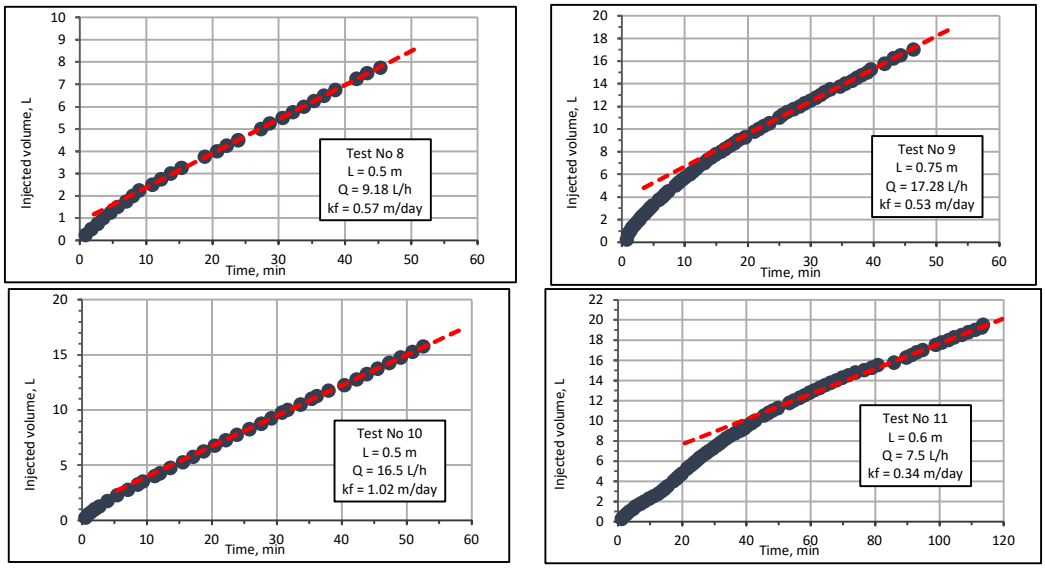

Figure 15. Filtration coefficients of near-surface sedimentary deposits derived from field tests.

When calculating the water balance of the study area, one of the key missing parameters is evapotranspiration. Evapotranspiration represents the combined process of moisture loss from the land surface to the atmosphere, including two interrelated components: the physical evaporation of water from soil surfaces, water bodies, and vegetation (evaporation), as well as transpiration—the release of water vapor from plant surfaces during their physiological activity.

This parameter is a critical component of the water balance, since in agroecosystems a significant portion of water losses is attributed to evapotranspiration. Under irrigated agriculture conditions, evapotranspiration is directly influenced by the biological characteristics of cultivated crops, their growth stages, temperature regime, solar radiation, wind speed, and air humidity. Neglecting this parameter may lead to significant errors in estimating infiltration recharge, drainage runoff, and groundwater replenishment.

To obtain spatially distributed evapotranspiration values, the capabilities of the Google Earth Engine (GEE) platform were used. GEE enables the processing of large volumes of satellite data and the generation of evapotranspiration maps that account for spatial heterogeneity across the study area.

Within this study, a thematic evapotranspiration map was generated based on satellite data using appropriate calculation algorithms. The obtained values made it possible to assess the spatial distribution of moisture loss across the study area, refine water balance parameters, and improve the accuracy of calculations related to infiltration and managed aquifer recharge.

- Google Earth Engine processing workflow.

Evapotranspiration (ET) represents one of the main output components of the hydrological and groundwater balance, reflecting water loss from the land surface through evaporation and plant transpiration. In this study, multi-year average evapotranspiration was estimated using satellite data from the MODIS evapotranspiration product MOD16A2 (Collection 6.1). This dataset provides global evapotranspiration estimates at a spatial resolution of 500 m and a temporal resolution of 8 days, based on the Penman–Monteith approach, which integrates satellite-derived vegetation parameters with meteorological inputs.

The analysis was conducted using the Google Earth Engine cloud computing platform. The boundary of the study area was used as the region of interest (ROI). The evapotranspiration time series was analyzed for the period 2014–2024, defined in the script by specifying the start and end years and generating a sequence of annual intervals (Figure 16).

 doi:10.20944/preprints202604.1713.v1

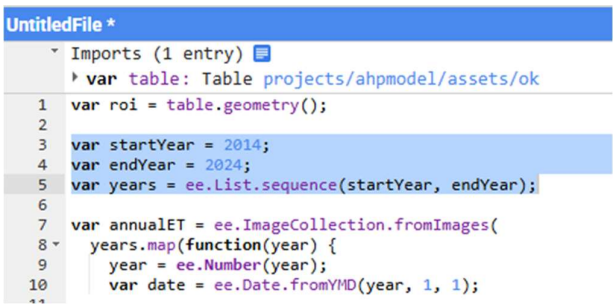

Figure 16. Google Earth Engine script for defining the study period and evapotranspiration dataset selection.

For each year within this period, the MOD16A2 evapotranspiration dataset was filtered by date and the ET band was selected for further analysis (Figure 17):

Figure 17. Extraction of annual evapotranspiration data (MOD16A2) within Google Earth Engine.

The MOD16A2 evapotranspiration values are provided in kg m^{-2} per 8-day period, which corresponds to millimeters of water depth. A scale factor of 0.1 was applied to convert the data to millimeters. Annual evapotranspiration was calculated by summing all 8-day ET values within each year (Figure 18):

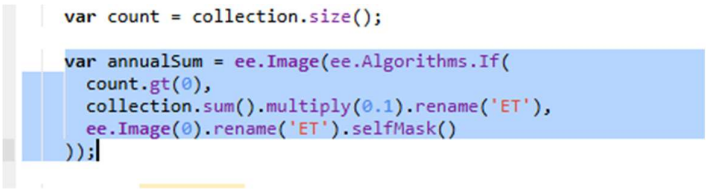

Figure 18. Calculation of annual evapotranspiration by summing 8-day ET values.

Subsequently, the multi-year average evapotranspiration was derived by calculating the mean of annual ET values for the entire study period (Figure 19):

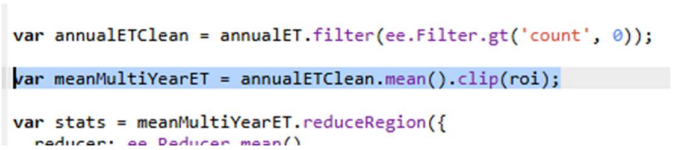

Figure 19. Computation of multi-year average evapotranspiration for the study area.

Spatial statistics of evapotranspiration were calculated for the study area using spatial averaging at a resolution of 500 m (Figure 20):

 doi:10.20944/preprints202604.1713.v1


```
var stats = meanMultiYearET.reduceRegion({
  reducer: ee.Reducer.mean(),
  geometry: roi,
  scale: 500,
  maxPixels: 1e13
});
```

Figure 20. Spatial statistics of evapotranspiration derived from multi-year averages.

The resulting dataset represents the spatial distribution of multi-year average evapotranspiration (mm/year). These values were used as one of the output components of the water balance analysis of the study area(Figure 24a).

The runoff coefficient was estimated using a spatially distributed multi-criteria approach implemented in Google Earth Engine. The catchment boundary was defined as a vector Feature Collection and used as the area of interest for all spatial analyses.

The estimation was based on the integration of key factors controlling surface runoff generation, including terrain slope, land use/land cover, soil properties, and vegetation conditions. Slope was derived from the SRTM digital elevation model. Land use/land cover information was obtained from the ESA World Cover dataset (2021). Vegetation conditions were represented by the Normalized Difference Vegetation Index (NDVI), calculated from MODIS (MOD13Q1) data for the growing season (April–October). Soil properties were represented by soil texture classes derived from the Open Land Map database.

Each factor was reclassified into a runoff potential scale ranging from 1 (low runoff potential) to 5 (high runoff potential). Slope classes were defined to reflect increasing runoff generation with increasing terrain steepness. NDVI values were interpreted inversely, where higher vegetation density corresponds to lower runoff potential. Land use/land cover classes were assigned scores based on their permeability and surface characteristics, while soil textures were grouped according to their relative permeability and infiltration capacity.

To ensure comparability, all factors were normalized to a 0–1 range. The layers were then integrated using a weighted overlay approach, where the weights reflect the relative importance of each factor in runoff generation processes (Figure 21).

```
/* ========================
   3. INPUT DATASETS
   ======================== */

// SRTM DEM (90 m), elevation band
var dem = ee.Image('CGIAR/SRTM90_V4').select('elevation').clip(AOI);

// Slope in degrees
var slope = ee.Terrain.slope(dem).clip(AOI);

// ESA WorldCover 2021 v200, band: Map
var lulc = ee.ImageCollection('ESA/WorldCover/v200').first().select('Map').clip(AOI);

// MODIS MOD13Q1 v061 NDVI, 16-day, 250 m
// NDVI in this product uses scale factor 0.0001
var ndvi = ee.ImageCollection('MODIS/061/MOD13Q1')
  .filterDate(ndviStart, ndviEnd)
  .select('NDVI')
  .mean()
  .multiply(0.0001)
  .clip(AOI);

// OpenLandMap soil texture class, choose topsoil 0 cm layer: b0
var soilTexture = ee.Image('OpenLandMap/SOL/SOL_TEXTURE-CLASS_USDA-TT_M/v02')
  .select('b0')
  .clip(AOI);
```

Figure 21. Input data preparation for runoff potential analysis.

The weights were assigned as 0.30 for slope and soil, 0.25 for land use/land cover, and 0.15 for NDVI, reflecting their relative contribution to runoff generation (Figure 22).

```
// ---- Weighted overlay coefficients (must sum to 1) ----
var weights = {
  slope: 0.30,
  soil:  0.30,
  lulc:  0.25,
  ndvi:  0.15
};
```

Figure 22. Weight assignment for model parameters.

 doi:10.20944/preprints202604.1713.v1

The resulting runoff potential index represents the spatial variability of runoff generation conditions across the catchment and forms the basis for subsequent estimation of the runoff coefficient. This approach allows for a more realistic representation of hydrological processes by accounting for the combined influence of terrain, land cover, soil, and vegetation characteristics (Figure 23).

```
6. COMPOSITE RUNOFF POTENTIAL INDEX
========================= */
var runoffPotential = slope01.multiply(weights.slope)
  .add(soil01.multiply(weights.soil))
  .add(lulc01.multiply(weights.lulc))
  .add(ndvi01.multiply(weights.ndvi))
  .rename('runoff_potential');
```

Figure 23. Runoff potential calculation using weighted overlay.

These results were used as input for the water balance analysis, with the spatial distribution of the runoff coefficient shown in (Figure 24c).

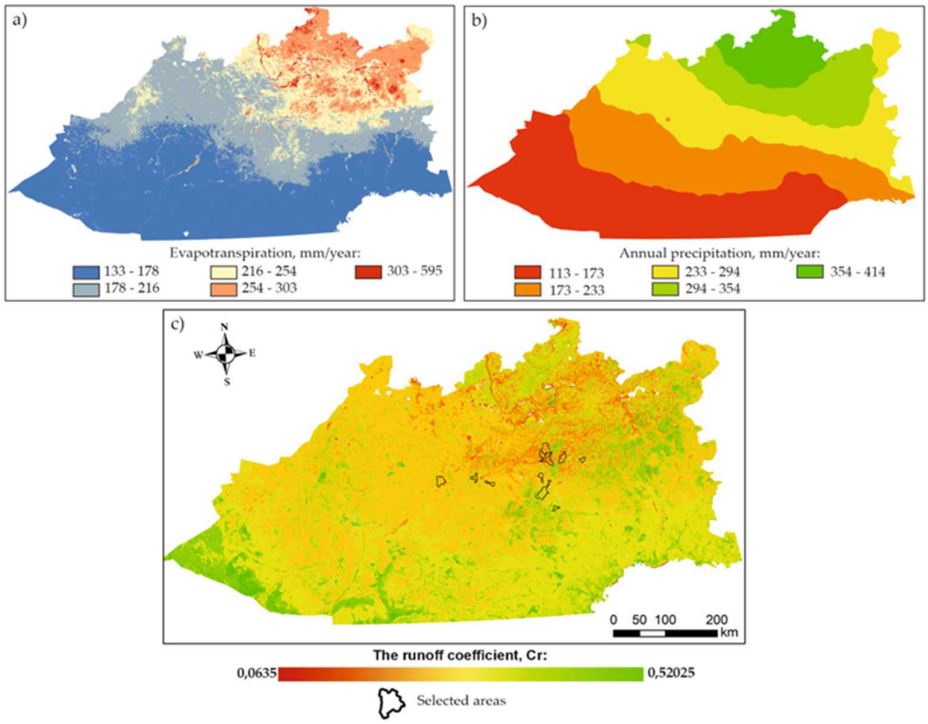

Figure 24. Integrated maps of evapotranspiration, precipitation, and runoff coefficient used for water balance analysis.

3. Results

Groundwater quality is one of the key factors determining the effectiveness of managed aquifer recharge (MAR) projects. Even when sufficient volumes of water are available for infiltration, the chemical composition of both the injected water and the receiving aquifer largely controls the sustainability and long-term performance of such interventions. Mismatches in hydrochemical characteristics can trigger various geochemical processes within the aquifer, including mineral dissolution or precipitation, which may alter groundwater composition and reduce the permeability of the filtering medium. In addition, the introduction of water with elevated concentrations of dissolved salts, nutrients, or trace elements may lead to gradual deterioration of groundwater quality and limit its suitability for drinking water supply, irrigation, and other uses.

Under the conditions of the study area, the implementation of MAR may serve not only to augment water resources but also to reduce the risk of soil salinization. The use of fresh water for

 doi:10.20944/preprints202604.1713.v1

infiltration promotes the dilution of mineralized groundwater and contributes to the establishment of a favorable hydrogeochemical regime in the vadose zone and upper aquifers. As fresh water enters the aquifer system, the concentration of dissolved salts decreases, reducing their accumulation in the soil profile and limiting the capillary rise of saline water to the surface.

Moreover, the infiltration of fresh water facilitates the gradual leaching of easily soluble salts from the upper soil horizons and unconsolidated deposits. This is particularly important in arid regions, where secondary salinization processes are often associated with shallow, mineralized groundwater. Thus, the use of fresh water for MAR creates conditions that not only enhance groundwater storage but also improve the hydrogeochemical state of soils, ultimately increasing the sustainability of agro-landscapes and the efficiency of water use.

Fieldwork also included sampling for chemical analysis of all identified groundwater sources, including wells, boreholes, and springs. Based on the obtained data on groundwater chemical composition, a map of the spatial distribution of mineralization was developed, reflecting the formation of hydrogeochemical halos. The cartographic model demonstrates the gradation of mineralization: fresh waters with mineralization up to 1 g/L are shown in light blue, slightly saline waters with mineralization ranging from 1 to 1.5 g/L are shown in blue, and waters with mineralization from 1.5 to 4 g/L are represented in dark blue. The map was generated using spatial analysis methods in ArcGIS, specifically through interpolation techniques, which made it possible to identify patterns in mineralization distribution and delineate zones of elevated values (Figure 25).

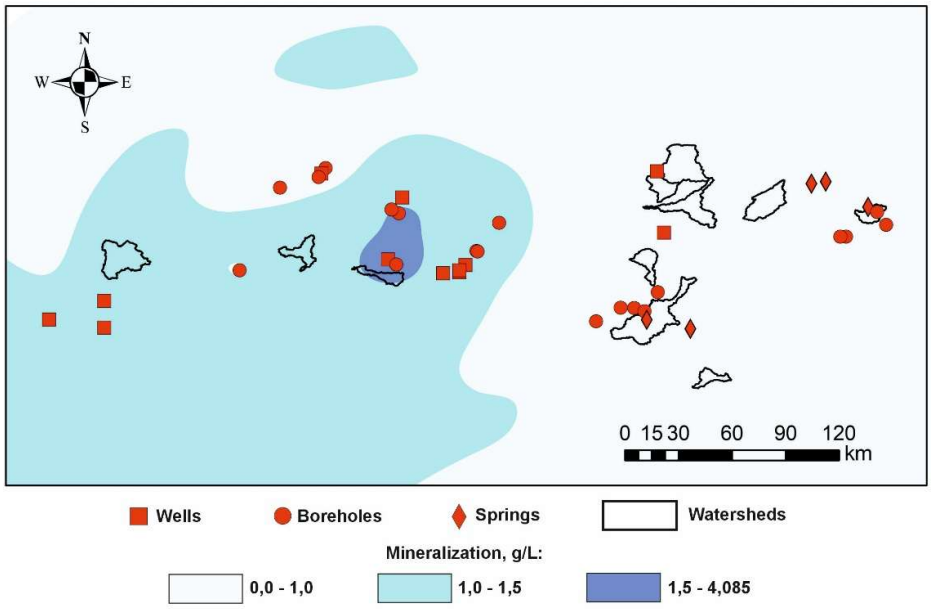

Figure 25. Map of groundwater mineralization distribution and sampling points.

Hydrochemical facies, presented on the Piper diagram (Figure 26), shows that groundwater in the study area predominantly belongs to the Ca–HCO_3 type, with a local transition to a mixed Na–Ca–HCO_3 type. Such a hydrochemical composition is typical of active recharge zones and indicates the dominance of atmospheric precipitation infiltration and water–carbonate rock interactions [43].

Low concentrations of chlorides and sulfates suggest the absence of significant influence from evaporite formations and intensive evaporation processes, indicating a low degree of hydrochemical evolution of groundwater [44]. This represents a favorable condition for the implementation of managed aquifer recharge (MAR) measures [45].

The range of total dissolved solids (TDS) shows that most samples correspond to fresh and slightly mineralized waters, meeting the requirements for aquifers suitable for MAR. These conditions indicate good hydrochemical compatibility between infiltrating water and the aquifer

 doi:10.20944/preprints202604.1713.v1

medium, reducing the risk of secondary geochemical processes such as mineral precipitation, salinization, or water quality deterioration.

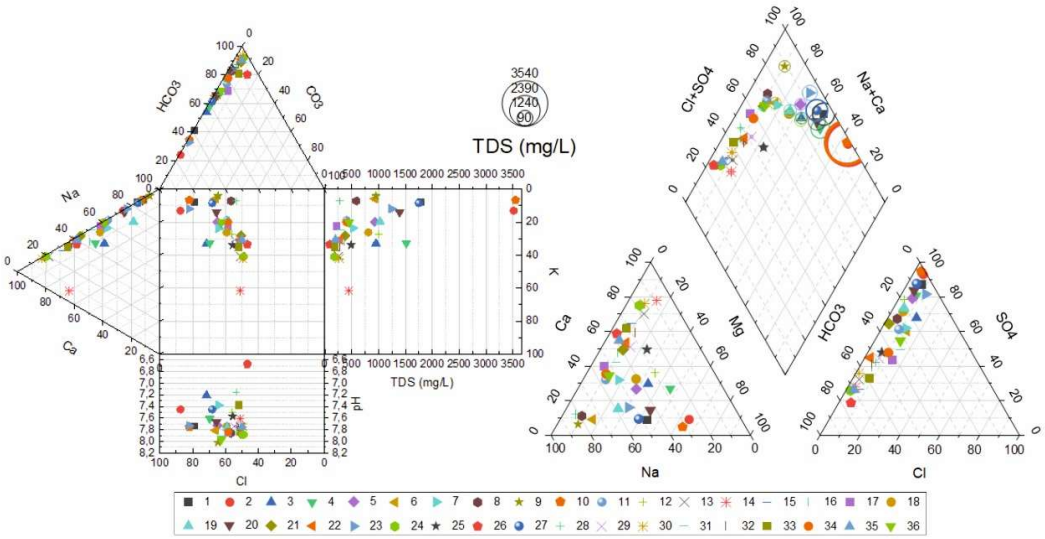

Figure 26. Hydrochemical facies classification based on the Piper diagram. 1- hole №2; 2- hole Shalkonyr; 3- hole Bidaiyk; 4- hole №1 Orynbai; 5- hole №2 Orynbai; 6- well №1 Kyryk kudyk; 7- well №2 Kyryk kudyk; 8- well №3 Kyryk kudyk; 9-well Kaksal; 10- hole Jan-baba; 11- hole Bayanbai bulak; 12- well Taldy bulak; 13- hole Shugy; 14- well №1 Kargaly; 15- well №2 Kargaly; 16- hole №2 Zhartas; 17-hole Karsyadyr; 18- well №2 Jenis; 19- well Tokty kora; 20- well Kyzyl jar; 21- spring Aksu-Ayuly; 22- hole №1 Aksu-Ayuly; 23- hole №2 Aksu-Ayuly; 24- hole №3 Aksu-Ayuly; 25- hole №4 Aksu-Ayuly; 26- spring №1 Tumsyk; 27- spring №2 Tumsyk; 28- well Burma; 29- well Uspenskyi; 30- hole Uspenskyi; 31- spring №1 Agadyr; 32- hole Orda; 33- hole №1 Agadyr; 34- hole №2 Agadyr; 35- hole №3 Agadyr; 36- spring №2 Agadyr.

In addition, slightly alkaline pH values (7.2–8.1) indicate stable geochemical conditions within the water–rock system and the absence of aggressive waters, which is also an important factor in MAR planning.

Thus, the results of the hydrochemical analysis confirm that the studied aquifer possesses favorable geochemical conditions for the implementation of MAR technologies, and the identified hydrochemical facies correspond to systems with active natural recharge and relatively young hydrogeochemical evolution.

To assess the potential for managed aquifer recharge (MAR), the following input data were used: annual precipitation, annual evapotranspiration, catchment area, runoff coefficients, runoff capture efficiency coefficients, hydraulic conductivity, aquifer thickness, hydraulic gradients within the catchments, and effective porosity.

At the first stage, the volume of water that can be collected from precipitation within each catchment was estimated. The calculation was performed as:

$$V_{capture} = \frac{P}{1000} \cdot A \cdot C_r \cdot \eta_c \quad (3)$$

where $\boldsymbol{P}$is annual precipitation (mm), $\boldsymbol{A}$is the catchment area (m²), $\boldsymbol{C_r}$is the runoff coefficient [46, 47], and $\boldsymbol{\eta_c}$is the runoff capture efficiency coefficient. This step provided the total volume of water potentially accumulated in each storage basin. This step provided the total volume of water potentially accumulated in each storage basin. If the dam is favorably located and a first-order approximation is considered, the coefficient can be taken as η_s = 0.7–0.9 as an engineering estimate. In hydraulic engineering design practice, however, it is recommended to adopt lower values of this

 doi:10.20944/preprints202604.1713.v1

coefficient to account for unfavorable conditions and uncertainties in the input data, especially in the absence of detailed observations [48].

At the second stage, the water surface area corresponding to the calculated storage volume was determined using a digital elevation model (DEM) in ArcGIS. The 3D Analyst – Surface Volume tool was applied to iteratively define the water level that matches the calculated storage volume. As a result, the water surface area (A_{pond}) was obtained for each site.

$$V_{ET} = \frac{ET}{1000} \cdot A_{pond} \quad (4)$$

At the third stage, evaporation losses from the ponded water surface were estimated as:

$$V_{available} = V_{capture} - V_{ET} \quad (4)$$

where $ET$is annual evapotranspiration (mm), and $Apond$is the water surface area (m²). The volume of water available for infiltration was then calculated as:

$$V_{capture} = \frac{P}{1000} \cdot A \cdot C_r \cdot \eta_c \quad (5)$$

Thus, the water balance at this stage included the collected runoff as input and evaporation losses as the primary output component.

At the fourth stage, the storage capacity of the receiving aquifer was evaluated to determine whether it can accommodate the infiltrated water:

$$V_{storage} = A_{pond} \cdot m \cdot n_e \quad (6)$$

where m is the aquifer thickness (m) and $n_e$is the effective porosity. This parameter was used as a verification criterion to assess whether the aquifer has sufficient available pore space.

At the fifth stage, the volume of water that can infiltrate into the aquifer was estimated based on Darcy's law:

$$V_{inf} = k_f \cdot i \cdot A_{pond} \cdot t \cdot C_F \quad (7)$$

where $k_f$is the hydraulic conductivity (m/day), $i$is the hydraulic gradient, $A_{pond}$is the infiltration area (assumed equal to the water surface area), $t$is the duration of water presence (days), and $C_F$is the clogging factor accounting for reduction in infiltration capacity. In this study, the duration $t$was assumed to be 365 days.

Finally, the effective recharge volume was determined as:

$$V_{recharge} = \min (V_{available}, V_{inf}) \quad (8)$$

The aquifer storage capacity ($V_{storage}$) was used as a validation parameter. In cases where $V_{storage} > V_{inf}$, the aquifer capacity was considered sufficient, and thus did not limit the MAR process. Under these conditions, the effective recharge was controlled primarily by water availability and infiltration capacity (Table 2).

 doi:10.20944/preprints202604.1713.v1

Table 2. Calculations for MAR Assessment.

Polygon number	m, m	k_f, m/day	V_{runoff}, m³	$V_{capture}$, m³	V_{ET}, m³	$V_{available}$, m³	V_k, m³	$V_{storage}$, m³	$V_{recharge}$, m³
1	5	0,41	2 747 461	1 923 223	167 802	1 755 421	18 592 904	1 308 594	**1 308 594**
2	5	0,26	10 517 415	7 362 190	1 343 521	6 018 669	11 550 570	10 230 657	**6 018 669**
3	8	0,72	4 821 059	3 374 741	503 304	2 871 437	32 728 049	6 219 198	**2 871 437**
4	4	0,57	3 246 039	2 272 228	423 272	1 848 956	77 814 930	2 382 857	**1 848 956**
5	5	1,02	9 670 302	6 769 211	533 921	6 235 291	168 905 160	3 323 454	**3 323 454**
6	9	0,34	5 3899 554	3 772 688	473 331	3 299 356	13 754 019	4 958 190	**3 299 356**
7	6	0,1	9 945 246	6 961 672	768 634	6 193 038	61 726 922	5 402 585	**5 402 585**
8	8	0,53	14 482 317	10 137 622	1 091 907	9 045 715	45 918 511	10 230 657	**9 045 715**
9	5	0,67	3 789 290	2 652 503	359 209	2 293 295	161 664 682	2 400 529	**2 293 295**
10	10	1,42	4 396 699	3 077 690	426 628	2 651 062	188 229 965	6 199 427	**2 651 062**
11	7	0,05	16 783 535	11 748 475	789 204	10 959 271	26 055 394	8 108 356	**8 108 356**

After assessing the suitability of the territory for Managed Aquifer Recharge (MAR) technologies and estimating the potential reservoir volumes, it is necessary to evaluate the infiltration recharge of the aquifer.

The infiltration volume was determined using the classical hydrogeological relationship:

$$V = k_f \cdot F_{inf} \cdot i \cdot t \quad (9)$$

where filtration properties of the geological formations, infiltration area, hydraulic gradient, and time are considered. This calculation made it possible to estimate the theoretical volume of water that can enter the aquifer under given conditions.

It is well understood that under real conditions, the filtration capacity of soils decreases over time due to clogging (colmation) processes caused by pore space blockage from suspended particles, chemical precipitates, and biological activity. Experimental and modeling studies show that hydraulic conductivity may decrease by 20–40% or more, in some cases significantly limiting infiltration [49–51]. Therefore, in engineering calculations, reduction coefficients are commonly introduced to account for clogging effects, especially in the absence of long-term observations. In this study, an average coefficient of 0.5, typical for sands and sandy loams, was adopted, allowing for a more realistic estimation of the actual infiltration volume.

As a result, the analysis transitioned from potential system characteristics to a more realistic assessment of its performance, taking into account natural constraints and operational factors (Table 3).

Table 3. Infiltration volume calculation.

Polygon number	k_f, m/day	i	F_{inf}, m²	t, day	CF	V_{inf}, m³	Q, m³/day
1	0,41	0,002	872 396	365	0,5	130 554	357,68
2	0,26	0,0028	7 157 457	365	0,5	950 940	2 605,31
3	0,72	0,003	2 591 333	365	0,5	1 021 503	2 798,64
4	0,57	0,003	1 985 714	365	0,5	619 692	1 697,79
5	1,02	0,0027	2 215 636	365	0,5	1 113 590	3 050,93
6	0,34	0,002	1 836 367	365	0,5	227 893	624,36
7	0,1	0,0021	3 001 436	365	0,5	115 030	315,15
8	0,53	0,0032	4 262 774	365	0,5	1 319 414	3 614,83
9	0,67	0,0018	1 600 3653	365	0,5	391 366	1 072,24
10	1,42	0,0036	2 066 476	365	0,5	1 927 898	5 281,91
11	0,05	0,0018	3 861 122	365	0,5	63 419	173 75

 doi:10.20944/preprints202604.1713.v1

4. Discussion

The new findings considerably narrow the knowledge gap on the MAR potential in the study region, and the need to include progressive infiltration modeling in recharge estimations. The recalculated values demonstrate that the overall effective recharge (approximately 11.0 million m 3/year) is much greater than the estimated one (5.09 million m 3/year) in the past, which means that the infiltration capacity was underestimated in the past.

Although this has increased, there is still an apparent imbalance between the water availability (~40.2 million m3/year) and the actual water recharge with the contribution of available water to groundwater recharge being only about 27%. This validates the fact that infiltration processes continue to remain the main limiting factor that regulates MAR efficiency in the area. The revised ratio, however, indicates that, given good hydrogeological circumstances, much greater amounts of surface runoff can be used productively than thought before.

The spatial diversity of recharge rates, which ranges between less than 200 m^3 /day to over 5,000 m^3 /day, proves that the performance of MAR is very location-specific and heavily relies on the hydraulic conductivity, infiltration area, and local gradients. Sites with greater permeability and bigger infiltration areas contribute dis-proportionately to the overall recharge volume, and, therefore, proper site selection is essential.

Notably, the evaluation of the storage capacity in the aquifers proves that V storage is greater than V inf in all the appropriate locations, meaning that subsurface storage is not a constraining element. This observation verifies that small-scale MAR systems that use retention dams can be implemented without a fear of overloading the aquifer capacity.

Simultaneously, there are still uncertainties related to the utilization of generalized parameters of hydraulic gradients, clogging coefficients, and climatic inputs. The lack of long-term monitoring information such as ground water level processes and on-site infiltration measures presents a possibility of variability in estimating recharge. Also, the local heterogeneity might not be fully reflected using remotely sensed precipitation and evapotranspiration data.

Future studies must thus be directed towards the deployment of monitoring infra-structure of piezometers and meteorological stations, and pilot-scale MAR experiments to test the assumptions of the models and parameters to be optimized. The results would also be more robust with incorporating the uncertainty analysis (e.g., sensitivity testing or stochastic simulations).

5. Conclusions

This research indicates that multi-criteria analysis that is GIS-based, field-based hydrogeological parameters, and water balance (modeling) can be used to provide a reliable framework of identifying and assessing the potential of managed aquifer recharge (MAR) in arid Central Kazakhstan. Hydrochemical studies have shown that 8 of the 11 chosen locations are suitable to implement MAR which is predominantly fresh to slightly mineralized groundwater with good geochemical conditions to promote penetration. Quantitative evaluation shows that the total water to be recharged per year is about 40.2 million m3 and the effective recharge is about 11.0 million m^3/year. This is equal to a total recharge efficiency of about 27%, and this proves that the infiltration capacity though still limiting is much higher than previously anticipated. The aquifer storage capacity analysis has revealed that the pore volume exceeds the infiltration volumes in all locations, and storage limits are not restrictive to MAR implementation.

As a result, the processes of surface-subsurface interaction, such as hydraulic conductivity, infiltration area, and clogging dynamics, are the main factors controlling the recharge efficiency. The estimated rates of recharge between 174 to 5,282 m^3/day are evidence that the MAR sites identified can serve pasture-based water supply systems and enhance water availability in rural areas. In general, the outcomes validate that miniature retention dam-based MAR systems were the potential and feasible solution to improving the groundwater resources in the water-limited areas. The suggested methodology offers a regional planning tool that could be transferred to other regions and

 doi:10.20944/preprints202604.1713.v1

could be utilized to support decision-making processes to achieve sustainable water re-resource management and climate resilience.

Author Contributions: Zh.O.: conceptualization, methodology, calculations, and preparation of cartographic materials and figures; A.A.: data processing, field data analysis, and preparation of the manuscript text and figures; V.S. and A.J.: scientific consultation and expert guidance throughout the study; A.E. and D.E.: field investigations and data collection; Zh. O. and R.A.: writing—review and editing. All authors have read and agreed to the published version of the manuscript.

Funding: This research was funded by the Science Committee of the Ministry of Science and Higher Education of the Republic of Kazakhstan under the project "Development of Technologies for Man-aged Aquifer Recharge (MAR) for Water Supply of Settlements, Industrial Enterprises, and Pasture Watering in the Low-Hill Regions of Central Kazakhstan", grant No. AP23490816.

Data Availability Statement: The original contributions presented in this study are included in the article. Further inquiries can be directed to the corresponding author**.**

Conflicts of Interest: The authors declare no conflicts of interest.

References

1. Bilal, H.; Govindan, R.; Zekri, S.; Al-Maktoumi, A.; Rajabi, M.M.; Triki, C.; Harrathi, W.Identification of Potential Managed Aquifer Recharge Sites in Hyper-Arid Environment Using GIS and Analytical Hierarchy Process. Applied Water Science 2025, 15, 99. https://doi.org/10.1007/s13201-025-02431-3
2. Hadded, R.; Ben Zaied, M.; Castelli, G.; Abdelli, F.; Essifi, B.; Bresci, E.; Ouessar, M. Enhancing Groundwater Resources through Managed Aquifer Recharge: A SWAT Application in Arid Southeastern Tunisia. Journal of Hydrology: Regional Studies 2026, 63, 103027. https://doi.org/10.1016/j.ejrh.2025.103027
3. Cao, H.; Qian, J.; Chen, H.; Liu, C.; Gao, S.; Lyu, M.; Dong, W.; Hu, C. Managed Aquifer Recharge and Extraction Effects on Groundwater Level and Quality Dynamics in a Typical Temperate Semi-Arid Fissured Karst System: A Multi-Method Quantitative Study. Hydrology and Earth System Sciences 2025, 29, 5213–5231. https://doi.org/10.5194/hess-29-5213-2025
4. Al-Maktoumi, A. A Review of Factors Affecting the Performance and Impact of Managed Aquifer Recharge Projects: Insights from Arid Regions. *Journal of Groundwater Science and Engineering* 2025, *13*, 312–340. https://doi.org/10.26599/JGSE.2025.9280057
5. Korkut, M.; Hartog, N.; Yavuz, V. An Overview of Historical Development, Current Situation, and Future Prospects of Managed Aquifer Recharge in Türkiye. *Water* 2025, *17*, 439. https://doi.org/10.3390/w17030439
6. El Farchouni, A.; Hadri, A.; Fakır, Y.; Ouarani, M.; Azaroual, M.; Kchikach, A. Mapping Groundwater Recharge Potential Zones in a Semi-Arid, Anthropogenically Modified Mountainous Basin. *Scientific African* 2025, *30*, e03025. https://doi.org/10.1016/j.sciaf.2025.e03025
7. Stautzebach, J.; Steidl, J.; Merz, C. The Potential of Localized Near-Nature Managed Aquifer Recharge in the Context of Climate Change Adaption—An Assessment within Brandenburg's Lower Spree Catchment. *Groundwater for Sustainable Development* 2025, *31*, 101549. https://doi.org/10.1016/j.gsd.2025.101549
8. Yin, G.; Xu, X.; Li, T.; Wang, T.; Yen, H.; Hua, L.; Jiao, H.; Tong, B.; Du, X.; Wen, H.; Li, W. Interactions between Soil Water and Groundwater Differ during Artificial Recharge and Extreme Rainfall Periods. *Agricultural Water Management* 2025, *321*, 109944. https://doi.org/10.1016/j.agwat.2025.109944
9. Mavundla, K.P.; Okedi, J.; Kalumba, D.; Armitage, N.P. Estimation of Infiltration Parameters for Groundwater Augmentation in Cape Town, South Africa. *Hydrology* 2025, *12*, 87. https://doi.org/10.3390/hydrology12040087
10. Pirasteh, S.; Samad, A.; Ahmad, R.; Thakural, L.N.; Khan, H.H.; Chauhan, P.; Khan, A.; Qamar, M.Z. Geospatial and AHP Based Identification of Potential Zones for Groundwater Recharge in Haridwar District of India. *Frontiers in Environmental Science* 2025, *13*, 1421918. https://doi.org/10.3389/fenvs.2025.1421918

 doi:10.20944/preprints202604.1713.v1

11. Song, Q.; Liu, Y.; Wang, Z.; Xu, Z. Assessing Groundwater Artificial Recharge Suitability in the Mi River Basin Using GIS, RS, and FAHP: A Comprehensive Analysis with Seasonal Variations. *Applied Water Science* 2025, *15*, 39. https://doi.org/10.1007/s13201-025-02362-z
12. Arya, V.; Rao, M.S. Groundwater Recharge Potential Index and Artificial Groundwater Recharge in the Alluvial Soils of the Middle Ganga Basin. *Discover Applied Sciences* 2024, *6*, 367. https://doi.org/10.1007/s42452-024-05851-z
13. Jung, H.; Saynisch-Wagner, J.; Schulz, S. Can Explainable AI Offer a New Perspective for Groundwater Recharge Estimation?—Global-Scale Modeling Using Neural Network. *Water Resources Research* 2024, *60*, e2023WR036360. https://doi.org/10.1029/2023WR036360
14. Al-Ruzouq, R.; Shanableh, A.; Jena, R.; Mukherjee, S.; Khalil, M.A.; Gibril, M.B.A.; Pradhan, B.; Hammouri, N.A. Hybrid Deep Learning and Remote Sensing for the Delineation of Artificial Groundwater Recharge Zones. *The Egyptian Journal of Remote Sensing and Space Sciences* 2024, *27*, 178–191. https://doi.org/10.1016/j.ejrs.2024.02.006
15. Gururani, D.M.; Kumar, Y.; Abed, S.A.; Kumar, V.; Vishwakarma, D.K.; Al-Ansari, N.; Singh, K.; Kuriqi, A.; Mattar, M.A.
Mapping Prospects for Artificial Groundwater Recharge Utilizing Remote Sensing and GIS Methods. *Water* 2023, *15*, 3904. https://doi.org/10.3390/w15223904
16. Di Lena, F.; Berardi, M.; Masciale, R.; Portoghese, I. **Network** Dynamics for Modelling Artificial Groundwater Recharge by a Cluster of Infiltration Basins. *Hydrological Processes* 2023, *37*, e14876. https://doi.org/10.1002/hyp.14876
17. Zaresefat, M.; Derakhshani, R.; Nikpeyman, V.; GhasemiNejad, A.; Raoof, A.Using Artificial Intelligence to Identify Suitable Artificial Groundwater Recharge Areas for the Iranshahr Basin. *Water* 2023, *15*, 1182. https://doi.org/10.3390/w15061182
18. Kariyawasam, T.; Basnayake, V.; Wanniarachchi, S.; Sarukkalige, R.; Rathnayake, U.Application of GIS Techniques in Identifying Artificial Groundwater Recharging Zones in Arid Regions: A Case Study in Tissamaharama, Sri Lanka. Hydrology 2022, 9, 224. https://doi.org/10.3390/hydrology9120224
19. Epting, J.; Vinnå, L.R.; Piccolroaz, S.; Affolter, A.; Scheidler, S. Impacts of Climate Change on Swiss Alluvial Aquifers—A Quantitative Forecast Focused on Natural and Artificial Groundwater Recharge by Surface Water Infiltration. Journal of Hydrology X 2022, 17, 100140. https://doi.org/10.1016/j.hydroa.2022.100140
20. Ousrhire, A.; Ghafiri, A.Artificial Aquifer Recharge: Systematic Mapping Study. Water Practice and Technology 2022, 17, 1706–1727. https://doi.org/10.2166/wpt.2022.082
21. Bogomolov, Y.G.; Abdulkerimov, F.G.; Dashtiev, Z.K.; Nikolaev, A.P. On the Possibility of Artificial Recharge of Groundwater Resources in the Territory of Derbent City. Proceedings/Conference Paper n.d., 166–167.
22. Belyakova, Y.V.; Solovyova, A.V.; Dymova, T.V.Ecological Methods of Artificial Recharge of Groundwater. Geology, Geography and Global Energy 2018, (2), 95–101
23. Jabassov, A.M.; Tukeshova, G.E.; Ermenbay, A.M.Application of Artificial Groundwater Recharge Technologies (Based on the Example of Aktobe Region). Science, New Technologies and Innovations of Kyrgyzstan 2024, (9), 30–34. https://doi.org/10.26104/NNTIK.2024.33.83.007
24. Petrishchev, V.P.; Leontieva, T.V.; Kudelina, I.V.Hydrogeological Technologies for Replenishing Water Bodies in the Eastern Orenburg Region. Geology, Geography and Global Energy 2020, (4), 89–94.
25. Zektser, I.S.; Potapova, E.Y.; Chetverikova, A.V.; Shtengelov, R.S.Prospects of Artificial Recharge of Groundwater in the South of the European Part of Russia. Water Resources 2012, 39(6), 624–638
26. Akhmetov, Z.; Iskakov, N. Review of the Monograph "Artificial Recharge of Groundwater in Arid Regions of Central Kazakhstan" by Zhaparhanov S.Zh. and Zhumataev B.K. Proceedings (KazNTU) 2012.
27. Yakovlev, E.Y.Analysis of Conditions for Artificial Recharge of Groundwater in Chuvashia. Advances in Current Natural Sciences 2013, (8), 66–67
28. Suleimanov, V.K.; Kurbanismailova, A.S. Artificial Recharge of Groundwater as a Method of Protection from Depletion. Proceedings of the Institute of Geology (Dagestan Scientific Center RAS) 2020, (4), 41–45. https://doi.org/10.33580/2541-9684-2020-83-4-41-45
29. Chetverikova, A.V.Groundwater of Russia: Artificial Recharge. Priroda 2015, (10), 29–31.

 doi:10.20944/preprints202604.1713.v1

30. Khalimov, D.P. International Experience of Artificial Recharge of Groundwater. Bulletin of KRSU 2016, 16(9), 142–143.
31. Leontieva, T.V.Methodological Issues of Hydrogeological Research and Justification of Groundwater Recharge Possibilities. Proceedings of Universities of Kyrgyzstan 2018, (2), 14–15
32. Degtyareva, O.G.; Degtyarev, V.G.Dams in the System of Regulation of Atmospheric Runoff on the Black Sea Coast of the Krasnodar Region. Monograph; KubSAU: Krasnodar, Russia, 2018; 164 p.
33. Em, T.; Amanzholova, R.; Rakhimov, T.; Musayeva, A. Alternative Solution for Aquifer Management and Application of Infiltration and Accumulation Methods in Agriculture. Geography and Water Resources 2025, (1), 56–68. https://doi.org/10.55764/2957-9856/2025-1-56-68.6
34. Khusnutdinova, A.F.; Muravyeva, M.D.Technologies for Replenishment of Freshwater Resources. Alfabuild 2017, 1(1), 146–156.
35. Khurgin, R.E.; Zubareva, O.N.; Efremov, R.V.Artificial Recharge of Groundwater for Water Supply Purposes. System Technologies 2022, (3), 102–103. https://doi.org/10.55287/22275398_2022_3_102
36. Dzhaksymuratov, K.M.; Agzamova, I.A.; Gulomkadirova, M.A.; Khasanov, N.M.Artificial Recharge of Groundwater Using Takyr Runoff in the Karakalpak Ustyurt Region. Proceedings (Central Asia) 2022.
37. Tsymbalov, A.A.Dynamics of Water Balance Impact on the Performance of Artificial Groundwater Recharge Systems in Unconfined Aquifers. Proceedings n.d., 129–130.
38. Li, M.; Liu, T.; Duan, L.; Luo, Y.; Ma, L.; Zhang, J.; Zhou, Y.; Chen, Z. The Scale Effect of Double-Ring Infiltration and Soil Infiltration Zoning in a Semi-Arid Steppe. Water 2019, 11, 1457. https://doi.org/10.3390/w11071457
39. Rönnqvist, H. Double-Ring Infiltrometer for In-Situ Permeability Determination of Dam Material. *Engineering* 2018, *10*, 320–328. https://doi.org/10.4236/eng.2018.106022
40. Reynolds, W.D. Measuring Soil Hydraulic Properties Using a Cased Borehole Permeameter: Falling-Head Analysis. *Vadose Zone Journal* 2011, *10*, 999–1015. https://doi.org/10.2136/vzj2010.0145
41. Angulo-Jaramillo, R.; Bagarello, V.; Iovino, M.; Lassabatère, L. Infiltration Measurements for Soil Hydraulic Characterization. *Cambridge International Law Journal* 2016.
42. Al-Yaqout, A.F. In Situ Hydraulic Conductivity Tests for Compacted Calcareous Sands Using Sealed Double Ring Infiltrometers (SDRI). *Journal of Engineering Research* 2016, *4*(1), 65–83. https://doi.org/10.1016/S2307-1877(25)00876-4
43. Shiraki, S., Aung Kyaw Thu, Matsuno, Y. et al. Evaluation of infiltration models and field-saturated hydraulic conductivity in situ infiltration tests during the dry season. *Paddy Water Environ* 17, 619–632 (2019). https://doi.org/10.1007/s10333-018-00688-w
44. Nogueira, G.E.H.Tracing the Hydrochemical Water Types and Salinization Mechanisms in the Great Maputo Area as a Function of Groundwater Recharge, Hydrogeological Properties and Human Activities. *M.Sc. Thesis*, Instituto Superior Técnico, Universidade de Lisboa, Lisbon, Portugal, 2017
45. Marzouki, H.; Nordine, N.; Azzirgue, E.M.; Silva, J.C.G.E.d.; Cherif, E.K. From Contamination to Conservation: A Hydrochemical and Isotopic Evaluation of Groundwater Quality in the Semi-Arid Guire Basin (Morocco). Water 2025, 17, 1688. https://doi.org/10.3390/w17111688
46. García-Menéndez, O.; Renau-Pruñonosa, A.; Morell, I.; Ballesteros, B.J.; Esteller, M.V. Hydrogeochemical Changes during Managed Aquifer Recharge (MAR) in a Salinised Coastal Aquifer. *Applied Geochemistry* 2021, *126*, 104866. https://doi.org/10.1016/j.apgeochem.2020.104866
47. Liu, W.; Li, Z.; Zhu, J.; Xu, C.; Xu, X.Dominant Factors Controlling Runoff Coefficients in Karst Watersheds. *Journal of Hydrology* 2020, *590*, 125486. https://doi.org/10.1016/j.jhydrol.2020.125486
48. Itsukushima, R. Characteristics and Controlling Factors of the Drought Runoff Coefficient. Water 2021, 13, 1259. https://doi.org/10.3390/w13091259
49. Food and Agriculture Organization of the United Nations (FAO). Rainfall–Runoff Analysis. *FAO Irrigation and Drainage Paper No. 50*; FAO: Rome, Italy, 1991. Available online: https://www.fao.org/3/u3160e/u3160e05.htm
50. Zou, Z.; Shu, L.; Min, X.; Chifuniro Mabedi, E. Clogging of Infiltration Basin and Its Impact on Suspended Particles Transport in Unconfined Sand Aquifer: Insights from a Laboratory Study. Water 2019, 11, 1083. https://doi.org/10.3390/w11051083

 doi:10.20944/preprints202604.1713.v1

51. Zhang, H.; Ye, X.; Du, X. Laws and Mechanism of the Fe (III) Clogging of Porous Media in Managed Aquifer Recharge. Water 2021, 13, 284. https://doi.org/10.3390/w13030284
52. Todisco, F.; Vergni, L.; Ceppitelli, R. Modelling the Dynamics of Seal Formation and Pore Clogging in the Soil and Its Effect on Infiltration Using Membrane Fouling Models. *Journal of Hydrology* **2023**, *618*, 129208. https://doi.org/10.1016/j.jhydrol.2023.129208